International Journal of Rotating Machinery, 10(4): 233–240, 2004

ISSN: 1023-621X print / 1542-3034 online
DOI: 10.1080/10236210490447494

Taylor & Francis
Taylor & Francis Group

Proposition of Unique Pumping System with Counter-Rotating Mechanism

Toshiaki Kanemoto and Shin Oba
Kyushu Institute of Technology, Tobata, Kitakyushu, Japan

Turbo-pumps have weak points, such as when the pumping operation becomes unstable in the rising portion of the head characteristics and/or the cavitation occurs under the intolerably low suction head. To overcome both weak points simultaneously, this article proposes a unique pumping system with counter-rotating mechanism, which consists of two-stage impellers and a peculiar motor with double rotors. The front and the rear impellers are driven by the inner and the outer rotors of the motor, respectively, keeping the relative rotational speed constant and counter-balancing the rotational torque. Such driving conditions not only smartly improve the unstable performance at lower discharge, but also suppress the cavitation at higher discharge, in the optimum cooperation with the impeller works and the rotor outputs.

Keywords Cavitation, Counter-Rotation, Impeller, Motor, Pump, Unstable Performance

The operating condition of turbopumps may become unstable when the head characteristic curve has the rising portion and/or the cavitation occurs when the suction head is intolerably low. In an effort to overcome these unacceptable weak points, these phenomena and causes have been energetically investigated (Gopalakrishuman et al., 1999) and fruitful devices also have been proposed in the individual cases. For instance, the unstable operating condition can be suppressed well with the swirl-stop, the annular wing (Kaneko et al., 1990), or the additional jet flow along the suction cover just in front of the impeller inlet (Goto, 1994). Moreover, the inducer is best effective to protect the main impeller blade from the cavitation erosion (Kamijo, 1998). Both unacceptable weaknesses, however, have been individually investigated and generally overcome because they are induced from essentially different causes.

The authors have invented the unique pumping system with which the above weak points can be overcome simultaneously. In construction of system, the new type of AC induction motor with the counter-rotating rotors instead of the usual mechanism was developed. The inner and outer rotors drive the front and rear impellers, respectively, under the condition that the relative rotational speed between both rotors is kept constant and the rotational torque is counter-balanced. These two driving conditions play important parts in automatically optimizing the front and rear impeller works in response to the change of the pumping discharge. This action is called newly "smart control" by the authors.

This article gives the details of the counter-rotating type pumping system described above and expounds the mechanism of the smart control for simultaneously overcoming the unstable performance and cavitation. Moreover, the characteristics of the model impellers are numerically predicted, and the smart control of the pump performances is proved experimentally with the trial model system. The concept of the counter-rotation proposed in this article entirely differs from the conventional impellers (Kodama et al., 1994; Shigemitsu et al., 2002), ship propellers (Caricchi et al., 1994), etc., which are separately driven with the individual motors or engines.

COUNTER-ROTATING TYPE AC INDUCTION MOTOR

The counter-rotating type of AC induction motor (2-poles and 3-phases, 3.7 kW–200 V) was prepared for constructing the trial model of this unique pumping system. As shown in Figure 1, main parts of this model motor consist of the inner rotor and the outer rotor replacing the conventional stator. Moreover, the motor is equipped with the supplementary fan connected to the rear shaft of the inner rotor. The fan compensates to make the mechanical torque of the inner rotor shaft coincide well with that of the outer rotor shaft, in the no-load operation. The magnetomotive force due to the revolving electromagnetic field, which is induced from the outer rotor, makes both rotors counter-rotate successfully. Then, the relative rotational speed n_{MT} between the

Received 25 June 2002; accepted 1 July 2002.
Address correspondence to Toshiaki Kanemoto, Kyushu Institute of Technology, Sensui 1-1, Tobata, Kitakyushu 804-8550, Japan. E-mail: turbo@tobata.isc.kyutech.ac.jp

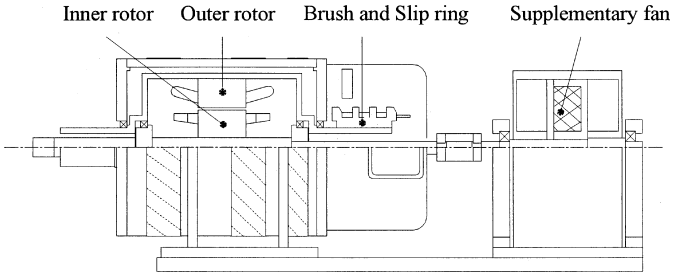

FIGURE 1
Counter-rotating type AC induction motor.

inner and the outer rotors ($= n_{MF} + n_{MR}$, where n_{MF} and n_{MR} are the individual rotational speed of the inner and the outer rotors, hereafter, ornamented here and there with "individual") is electrically determined by the power supply frequency f and the revolving slip (i.e., $n_{MT} = 3000\ \text{min}^{-1}$ at $f = 50$ Hz in the no-slip condition).

The relations of the counter-rotational torque between the inner and outer rotors are shown in Figure 2, when the load of the rotor is variously changed under the condition that the relative rotational speed n_{MT} is kept constant (3000, 2500, and 2000 min^{-1}) although the individual rotational speeds n_{MF} and n_{MR} are different. The torque of the inner rotor M_{MF} coincides with one of the outer rotor M_{MR}, regardless of the rotational speeds and/or the loads. This result surely proves that this motor is operated in the state when the rotational torque between the inner and outer rotors is counter-balanced. Accordingly, the counter-rotational torque is hereafter represented with nomenclature M_M. In addition, the combination of the individual rotational speeds n_{MF}, n_{MR} are arbitrary, even though the load (torque M_M) and the relative rotational speed n_{MT} are kept constant.

Figure 3 shows the relation between the output P_M and the rotational torque M_M, when the inner and outer rotor speeds

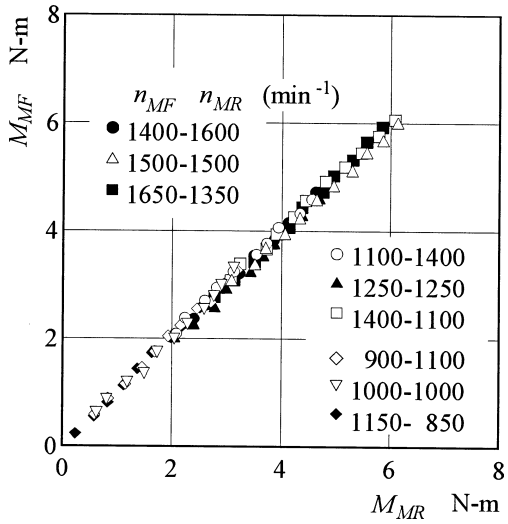

FIGURE 2
Counter-rotational torques of the inner and outer rotors.

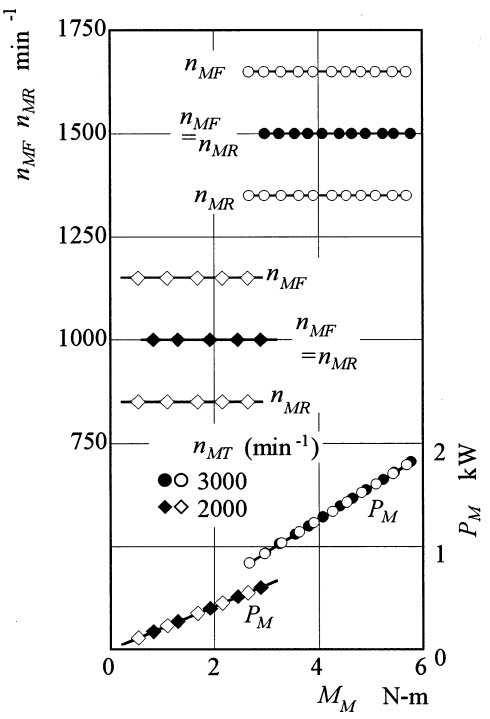

FIGURE 3
Characteristics of the motor (relative speed is kept constant).

n_{MF}, n_{MR} are changed, respectively, under the constant relative speed $n_{MT} = 3000$ and 2000 min^{-1}. The rotational speeds were carefully kept constant by means of the inverter control. It is confirmed that the difference of the individual speed never affects the output P_M proportional to the rotational torque M_M when only the relative speed n_{MT} is kept constant

$$[P_M = 2\pi(n_{MF} + n_{MR})M_M/60 = 2\pi n_{MT}M_M/60].$$

Discussions in the following sections are carried out under the premise that the relative rotational speed is constant, because the pump performances with the discharge control are evaluated at the constant impeller speed in general.

SMART CONTROL OF COUNTER-ROTATING IMPELLERS

The inner and outer rotors of the motor presented above can successfully and smartly counter-drive the front and rear impellers, in accordance with the above driving conditions that the rotational torque is counter-balanced and the relative rotational speed is kept constant. Figure 4 shows the velocity triangles in the ideal flow condition, where (a) is in the constant rotational speeds driven independently by the conventional motors and (b) is in the speeds controlled smartly by the counter-rotating type motor presented above. In this figure, u, v, and w, are the impeller speed, the absolute velocity, and the relative velocity, α and β are the absolute and the relative flow angles, and subscripts 1–4 denote the values at the impeller inlet and outlet

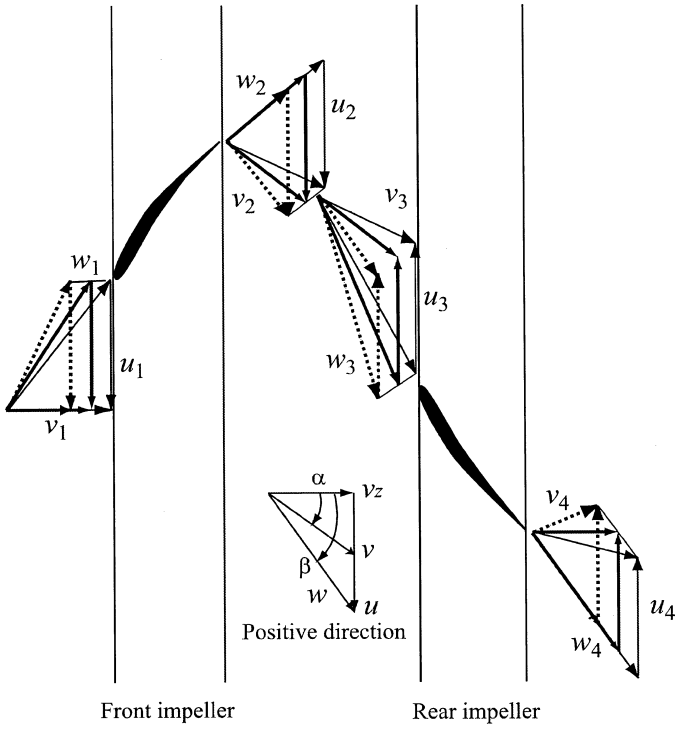

(a) In the constant speeds.

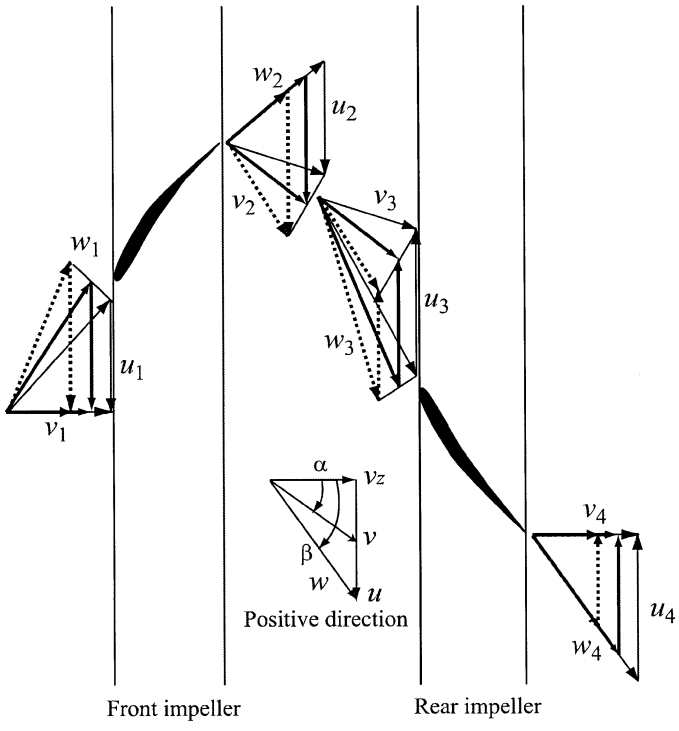

(b) In the smart control.

FIGURE 4
Velocity triangles through the axial flow type impellers (ideal flow condition).

sections, respectively. The flow directions α, not only at the front but also the rear impeller outlets, change in response to the pumping discharge when the front and rear impellers are independently driven by two conventional motors under the constant speeds (see Figure 4a). On the contrary, the impeller works are optimized with the counter-rotating type motor (see Figure 4b). That is, the inner and outer rotors automatically control the front and rear impeller speeds under the constant relative rotational speed, so as to make the rotational torque of the rear impeller coincide with that of the front impeller. Then, assuming the ideal flow condition and the axial flow at the front impeller inlet ($\alpha_1 = 0$), the flow must run to the axial direction at the rear impeller outlet ($\alpha_4 = 0$) irrespective of the discharge. This means that the angular momentum change through the rear impeller must coincide with the one through the front impeller in compliance with the demand of the rotors whose rotational torques are counter-balanced.

The thick-solid lines in Figure 4 give the velocity triangles of the design point presented in the next section, where the rotational speeds of the front and rear impellers are the same. When the pumping discharge is less than the design point (see the dotted lines in Figure 4), the rotational speed of the rear impeller in the smart control must decrease so as to get the axial flow at the outlet, namely, to make the angular momentum change coincide with that of the front impeller. Such rotating conditions also accompany with the increase of the front impeller speed in opposition to the decrease of the rear impeller speed, as the relative rotational speed must be kept constant. Then, the attack angle against the front impeller blade becomes large with the increase of the rotational speed, and the reverse flow, which may make the pump performance unstable, comes to occur at the entrance near the impeller tip in the actual flow condition with viscosity (Toyokura, 1960).

Such a reverse flow makes the rotational torque increase more than the angular momentum change through the front impeller. This additional torque of the front impeller plays to make the rear impeller speed increase, namely, to give the swirling flow component at the outlet as shown in Figure 5, because the rear impeller has to generate excessively the angular momentum change corresponding to the additional torque due to the reverse flow. Resultantly, the front impeller speed comes to decrease and the reverse flow is moderately suppressed in the lower discharge, because the increase of the rear impeller speed is related directly to the decrease of the front impeller speed under the operating condition that the relative rotational speed must be kept constant. Then, the pump head lowering in the front impeller comes to be successfully compensated by the head rising in the rear impeller with higher speed. These discussions suggest that this counter-rotating mechanism certainly contributes to making the pump performance stable in the lower discharge.

In the high discharge rather than the design point, the angular momentum change through the rear impeller becomes smaller than the one through the front impeller when both the impeller speeds are kept constant [see Figure 4a]. In the smart control,

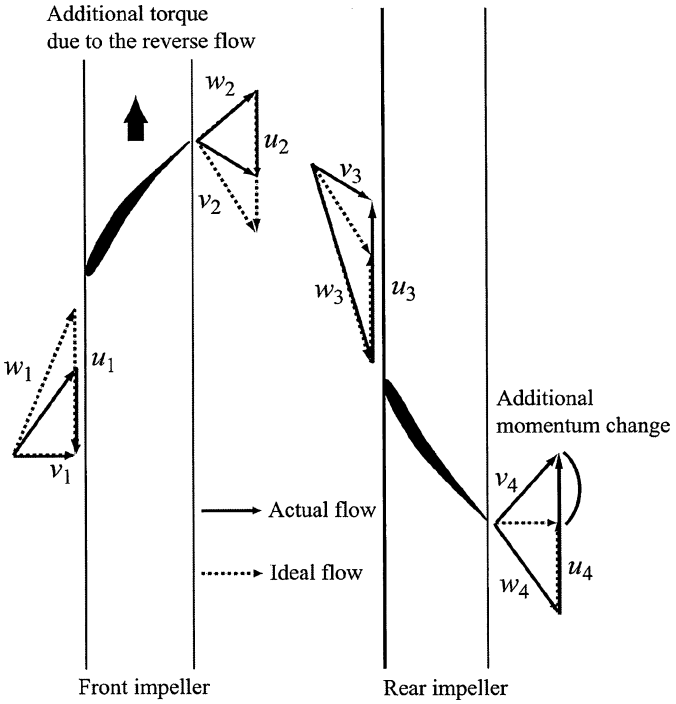

FIGURE 5
Velocity triangles in the smart control at lower discharge in the actual flow.

however, the rear impeller has to run faster than the front impeller for getting the swirl-less flow at the outlet (thin-solid lines in Figure 4b). It suggests that the front impeller takes place just like the inducer by means of the decrease of the rotational speed.

As discussed above, the proposed system has a fruitful peculiarity that the pump performances can be smartly controlled with the counter-rotating mechanism, which makes the rotational speeds of the front and rear impellers adjust automatically at the optimum operating condition. Moreover, it is not necessary to equip with the guide vanes (which makes the axial length of the machine longer), and it is not necessary to rigidly set up the motor because the rotational moment hardly acts on the mounting bed (self-balanced in the motor).

DESIGN OF MODEL IMPELLERS

In order to prove the smart control predicted in the preceding section, the following model impellers of the axial flow type were designed (JSME, 1971) assuming the axis-symmetrical ideal flow condition. At the design point; the theoretical head $H_{ET} = 4.4$ m, the discharge $Q_D = 1.78$ m^3/min, and the individual impeller speed $n_F = n_R = 1500\,\text{min}^{-1}$ (the subscripts F and R denote the front and rear impellers; the first subscript M in the preceding sections is removed hereafter). The specific speed of the individual impeller is $N_S = 1100$ (m, m^3/min, min^{-1}), and the specific speed as the pumping system is $N_{ST} = 1320$ (m, m^3/min, min^{-1}) which is estimated from the relative rotational speed $n_T (= n_F + n_R)$. The tip diameter of the impellers is 150 mm with the boss ratio 0.4. Taking material strength into consideration, the blade thickness derived from NACA4409 hydrofoil (Joseph et al., 1951) was distributed on the camber line of the single arc. The twist center was placed on the center of the camber line. The excess angle (Ikui, 1970) was taken into the outlet angle of the impeller blade to get the free vortex type flow at the front impeller outlet and the axial flow at the rear impeller outlet. The inlet angles of both blades were determined so as to get the shock-less condition. The numbers of the front and rear blades are 5 and 4, respectively, and the solidities of the both blades are 0.75 irrespective of the radial position.

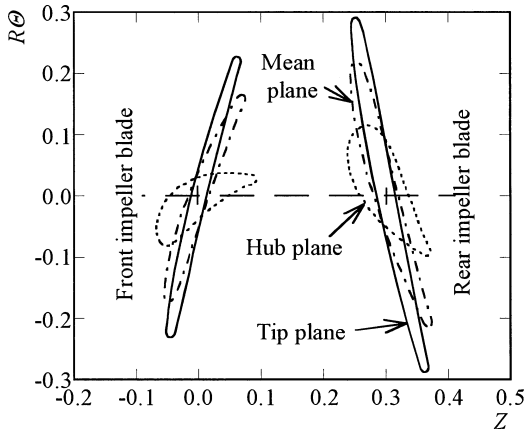

FIGURE 6
Blade profiles of the counter-rotating impellers.

The blade profiles designed above are shown in Figure 6 and Table 1, where $R\Theta$ and Z are the distances in the tangential (circumferential) and the axial directions divided with the impeller diameter, and β_D is the inlet and outlet angles of the blades measured from the axial direction (subscript numbers are referred to Figure 4).

PRESSURE PREDITION OF MODEL IMPELLER BLADES

The pressure distributions on the blade surfaces are shown in Figure 7, at the design point (normal operation point, discharge ratio $Q/Q_{D.} = 1$). These are predicted with the singularity method in the quasi-steady state condition (Kanemoto et al., 2000), where L is the dimensionless distance along the blade

TABLE 1
Blade angles and thickness

	Blade angle°				Maximum thickness (mm)	
	β_{d1}	β_{d2}	β_{d3}	β_{d4}	Front	Rear
Hub	−67.0	0.0	77.9	57.7	9.2 (39)	11.5 (38)
Mean	−77.4	−63.0	80.0	69.4	4.8 (43)	6.1 (41)
Tip	−80.4	−72.6	81.6	76.4	3.7 (46)	4.6 (43)

( ): station in percent of chord.

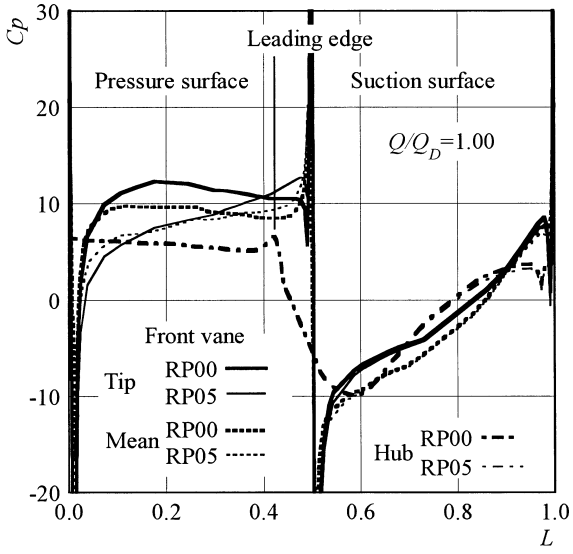

(a) Front blade.

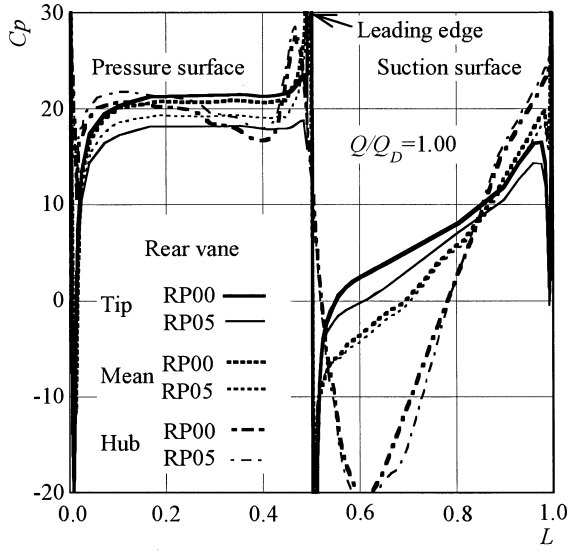

(b) Rear blade.

FIGURE 7
Pressure distributions on the blade surfaces at the design point.

surface measured from the trailing edge and C_P is the pressure coefficient based on the upstream static pressure and absolute velocity. In the prediction of the rear blade C_P, the theoretical head of the front impeller, which is averaged in the tangential direction, is taken into consideration. The abbreviation RP00 means that the tangential position of the rear blade center coincides with that of the front blade center, as shown in Figure 6, and RP05 means that the rear blade moved from the position of RP00 to the middle position of one pitch in the front blade row. The relative position between the front and rear blades naturally affects the pressure distributions, owing to the potential interference. The effect of the interference obviously appears on the opposite surfaces, namely, on the pressure surface of the

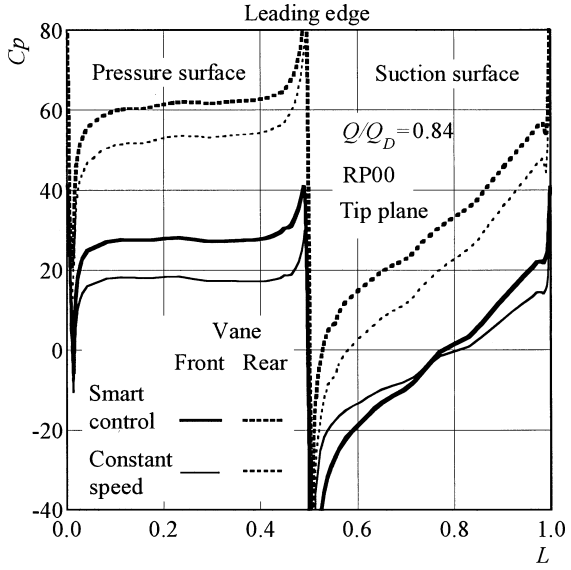

FIGURE 8
Comparison of pressure distributions with ones at constant speed.

front blade and the suction surface of the rear blade. The effect on the former surface is larger than that on the latter (see the thick and thin lines in Figure 7). The potential interference also affects the theoretical head (blade load), so that the C_P values of the rear blade including the effect of the front impeller head are changed with the relative position even though the distributions are similar profiles. Such effects discussed above, however, are not considered into the blade design and the data for the ideal operating conditions in the next section, as this article is in the first step to complete the pumping system of the counter-rotating type.

The pressure distributions at the low discharge ($Q/Q_D = 0.84$) were also predicted in comparison with ones in the constant speed condition, as shown in Figure 8. The thick lines "Smart control" are in the rotational speeds smartly controlled as given in Figures 4b and 9, that is, $n_F = 1737$ min^{-1} and $n_R = 1263$ min^{-1}. The thin lines "Constant speed" are in keeping the speeds constant $n_F = n_R = 1500$ min^{-1}, as given in Figure 4a. The blade load of the front impeller in the smart control is larger than the one in the constant speed at the low discharge, because the angular momentum change becomes large in accompany with the increase of the rotational speed. Then, the load and distribution of the rear impeller in the smart control scarcely differ from that in the constant speed, but the C_P values are affected with the front impeller load (theoretical head).

PERFORMANCE PREDICTION OF MODEL IMPELLERS

The impeller performances designed above were preliminarily estimated in the ideal operating condition, as shown in Figure 9, where H_E is the theoretical head, Q is the discharge, n_E is the individual rotational speed, and the second subscripts

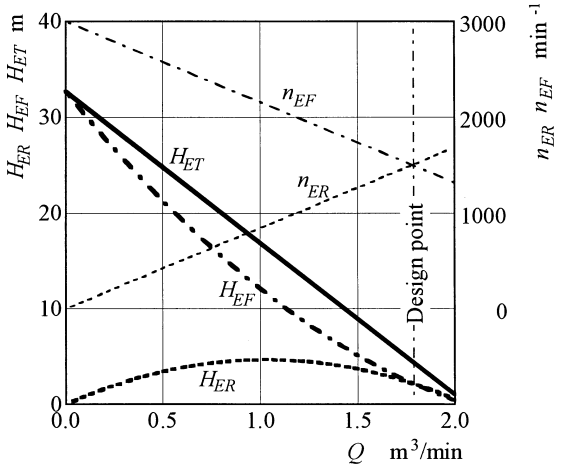

FIGURE 9
Impeller performances estimated in axis-symmetrical ideal flow condition.

F, R, and T denote the front, rear and counter-rotating impellers, respectively. As predicted before, the front impeller speed n_{EF} increases linearly and the rear impeller speed n_{ER} decreases linearly with the decrease of the discharge. Such speeds are smartly/automatically controlled under the optimum condition, as the angular momentum change through the front impeller coincides with one through the rear impeller. The individual impeller speeds controlled linearly make the theoretical head curves of H_{EF} and H_{ER} parabolic against the discharge, but the theoretical head of the counter-rotating impellers H_{ET} ($=H_{EF}+H_{ER}$) changes linearly the same as one of the conventional impeller with the constant rotational speed.

The total head H and the hydraulic efficiency η_h near the design point were also estimated at the impeller tip in the actual flow condition (Furukawa et al., 1999), and are shown in Figure 10 in comparison with the performances of the single-stage impeller which is designed conveniently under the same specifications N_{ST} at the rotational speed 3000 min^{-1}. The hydraulic loss of the counter-rotating type is less than one of the single type, and the efficiency is pretty good. In this figure, the required NPSH H_{SV} is also plotted at the design point, which is estimated when the coefficients for the relative and absolute velocity heads are 0.3 and 1.1. The head H_{SV} is improved markedly by means of the counter-rotation, and H_{SV} for the rear impeller becomes lower due to the pressure rising in the front impeller.

PERFORMANCES OF TRIAL MODEL PUMPING SYSTEM

To investigate experimentally the pump performances, the trial model of the pumping system was prepared as shown in Figure 11, which consists of the counter-rotating type impellers and the motor presented in Figures 6 and 1 (Kanemoto et al., 2002). The inner and outer rotors counter-drive directly the front and rear impellers, and each shaft is equipped with the lantern ring for choking the leakage flow.

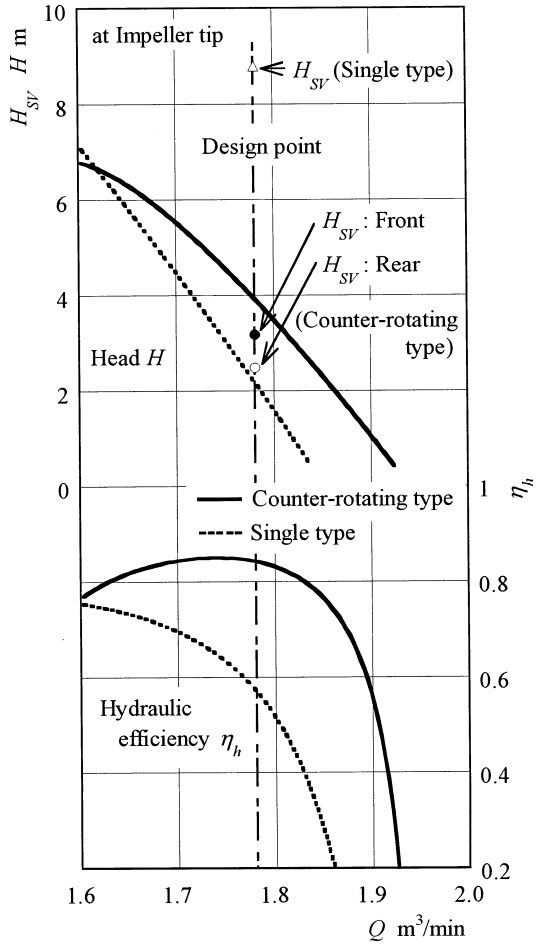

FIGURE 10
Impeller performances estimated in the actual flow condition.

Figure 12 shows the pumping characteristics of this system in keeping the relative rotational speed constant at $n_T = 3000$ min^{-1}. The pump head H_{WT} was estimated from the static pressure measured at the casing walls of Sections M0 and M5 (see Figure 11), P_I is the input power for the motor, and the total efficiency η_{PI} was obtained from $\rho g Q H_{WT}/P_I$. The input power scarcely increases irrespective of the decrease of the discharge as compared with the conventional pumps (Toyokura, 1960, 1963), and the maximum efficiency is obtained near the design point.

The individual rotational speeds n_F, n_R, and the head H_{WT} against the discharge Q behave just as predicted in the preceding section. That is, the front impeller speed n_F has the maximum value near $Q = 1.2$ m^3/min. The speed gradually becomes slow as the discharge increases from this point, and ultimately becomes slower than the rear impeller speed n_R where the discharge exceeds the design point. Such behavior may intimate that the smart control for the cavitation can be anticipated in the higher discharge by the proposed counter-rotating system.

To compare the head curve of the trial model with one of the conventional pump, Figure 13 shows the head curves of the usual

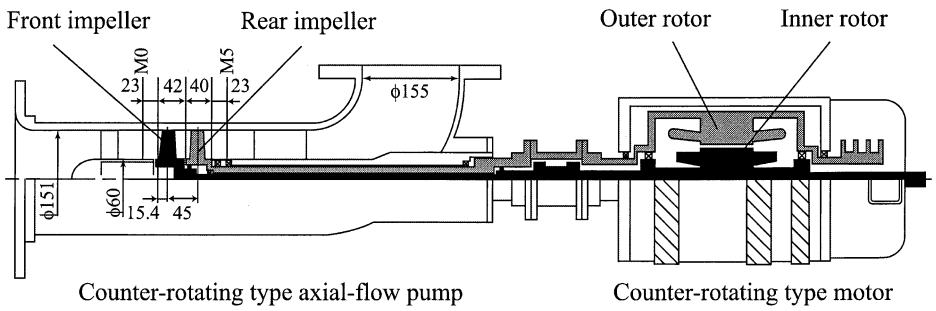

FIGURE 11
Trial model of the counter-rotating type pumping system.

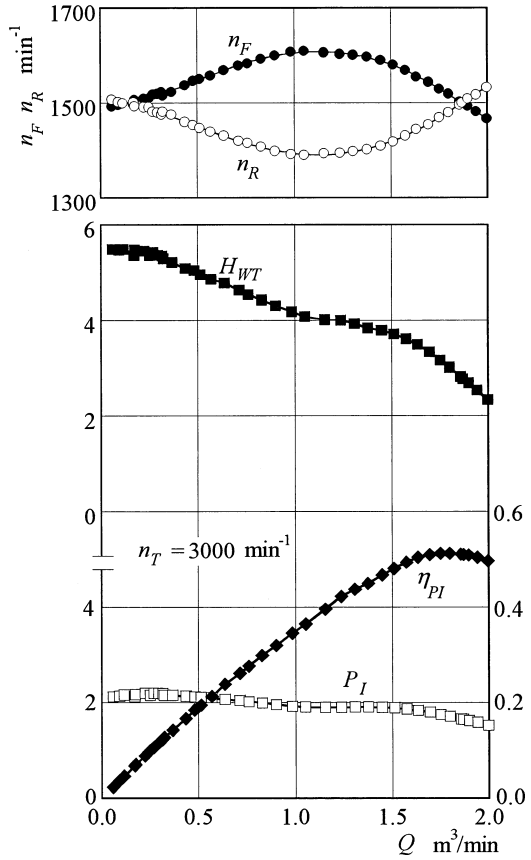

FIGURE 12
Pump performances of the trial model.

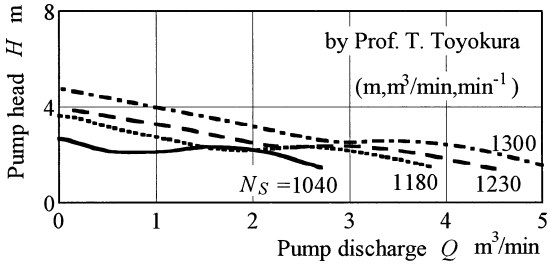

FIGURE 13
Head curves of conventional axial flow pumps.

axial flow pumps (Toyokura, 1963) composed of the single-stage impeller with nearly the same specific speed as N_S and/or N_{ST} of this trial model. It is obvious that the conventional pumps have the rising portion in the head curves. On the contrary, the proposed counter-rotating type never has the rising portion as recognized in Figure 12. This result suggests that the counter-rotating type pumping system in this article is also effective to improve smartly the unstable performance.

CONCLUSIONS

Turbo pumps have weak points, such as when the pumping operation becomes unstable in the rising portion of the head characteristics and/or the cavitation occurs under the intolerably low suction head. To overcome these weak points simultaneously, a unique pumping system with counter-rotating mechanism was proposed, which consists of the two-stage axial flow impellers and the peculiar motor with the double rotors. In the preliminary step, it was confirmed that the motor is operated in not only keeping the relative rotational speed constant but also counter-balancing the rotational torque. The impeller works were predicted and its prediction was verified experimentally with the trial model. The remarkable characteristics of the proposed pumping system are as follows.

(1) The front impeller accelerates and comes to decelerate automatically with the decrease of the discharge in keeping the relative speed constant. On the contrary, the speed of the rear impeller decreases and comes to increase with the decrease of the discharge.
(2) There is no rising portion in the head curve, and it can be expected to improve smartly the unstable performance by the proposed counter-rotating type.
(3) It can be, moreover, expected that the cavitation may also be suppressed smartly in the high discharge due to the decrease of the front impeller speed.

In the near future, the authors will propose the design data accompanying with the performances and the internal flow conditions in detail.

ACKNOWLEDGMENTS

The authors wish to thank Mr. S. Kimura and Ms. M. Sato, who graduated from Kyushu Institute of Technology, for helping with the experiments, and Dr. K. Yamamoto, Mr. N. Aoki, Dr. A. Goto, and Mr. M. Ishii of Ebara Research Co., Ltd. for kindly manufacturing the pumping system. This research was supported in part by the Harada Memorial Foundation in Japan and Satellite Venture Business Laboratory of Kyushu Institute of Technology.

REFERENCES

Caricchi, F. et al. 1994. Basic principle and design criteria of axial-flux PM machines having counter-rotating rotors. *Rec.1994 IEEE Ind. Appl. Conf.: 29th IAS Annu. Meet.* 247–253.

Furukawa, A. et al. 1999. Basic Study of a Contra-Rotating Axial Flow Pump Design and Pump Characteristics, 115–116 (in Japanese). *Proceedings of JSME in conference*.

Gopalakrishuman, S. et al. 1999. Pump research and development: past, present and future. *Transactions of the ASME Journal of Fluid Engineering* 121:237–258.

Goto, A. 1994. Suppression of mixed-flow pump instability and surge by the active alteration of impeller secondary flows. *Transactions of the ASME Journal of Turbomachinary* 116:621–628.

Ikui, T. 1970. *Fans and Compressors*, Asakura Publishing Co., Ltd. 239. (in Japanese).

Joseph, L. H. et al. 1951. Systematic two-dimensional cascade tests of NACA 65-series compressor blades at low speed. *NACA Tech. Note*, 3916.

JSME 1971. Pump design, 26, *JSME* (in Japanese).

Kamijo, K. 1998. Cavitation flows in pump inducers. *Turbomachinery* 26-3:161–168 (in Japanese).

Kaneko, K. et al. 1990. Passive control of unstable characteristics of a high specific speed diagonal-flow fan by an annular wing, *ASME Paper*, 90-GT-159, 1–7.

Kanemoto, T. et al. 2000. Discussion on numerical flow simulation for counter-rotating cascades, *Proceedings of the 5th International Symposium on Experimental And Computational Aerothermodynamics of Internal Flow*, 265–274.

Kanemoto, T. et al. 2002. Smart control of axial flow pump performance by means of counter-rotation. *JSME International J.* Series B, 45(2): 293–300.

Kodama, Y. et al. 1994. Experimental study on the characteristics of fluid dynamics and noise of a counter-rotating fan. *Transactions of the JSME* 60-576:2764–2779 (in Japanese).

Shigemitsu, T. et al. 2002. Experimental study on rear rotor design in contra-rotating axial flow pump. *Proceedings of the 5th JSME-KSME Fluid Engineering Conference*, Nagoya, OS16-2.

Toyokura, T. 1960. Studies on the characteristics of axial-flow pumps. *Transactions of the JSME* 26-168:1069–1324 (in Japanese).

Toyokura, T. 1963. Studies on the characteristics of axial-flow pumps, *Transactions of the JSME* 29-204:1318–1324 (in Japanese).